Journal of Catalysis 285 (2012) 92–102

Contents lists available at SciVerse ScienceDirect

Journal of Catalysis

journal homepage: www.elsevier.com/locate/jcat

Mechanistic interpretation of CO oxidation turnover rates on supported Au clusters

Manuel Ojeda [1], Bi-Zeng Zhan [2], Enrique Iglesia *

Department of Chemical Engineering, University of California and E.O. Lawrence Berkeley National Laboratory, Berkeley, CA 94720, United States

ARTICLE INFO

Article history:
Received 18 July 2011
Revised 13 September 2011
Accepted 14 September 2011
Available online 19 October 2011

Keywords:
CO oxidation
Au
H_2O effect
Mechanism
Hydroperoxy

ABSTRACT

Kinetic and isotopic data are used to interpret the mechanistic role of gaseous H_2O molecules and of non-reducible (Al_2O_3) and reducible (TiO_2, Fe_2O_3) supports on CO oxidation turnovers catalyzed by small Au clusters (<5 nm). H_2O acts as a co-catalyst essential for O_2 activation and for catalyst stability in CO oxidation at near-ambient temperatures, but also inhibits rates via competitive adsorption at higher H_2O pressures. The effects of CO, O_2, and H_2O pressures on CO oxidation turnover rates, the absence of $^{16}O_2/^{18}O_2$ and $^{16}O_2/H_2{}^{18}O$ exchange, and the small H_2O/D_2O kinetic isotope effects are consistent with quasi-equilibrated molecular adsorption of CO, O_2, and H_2O on Au clusters with the kinetic relevance of H_2O-mediated O_2 activation via the formation of hydroperoxy intermediates ($^*OOH$), which account for the remarkable reactivity and H_2O effects on Au clusters. These elementary steps proceed on Au clusters without detectable requirements for support interface sites, which are no longer required when H_2O is present and mediates O_2 activation steps. Rate enhancements by H_2O were also observed for CO oxidation on Pt clusters (1.3 nm), which is also limited by O_2 activation steps, suggesting H_2O-aided O_2 activation and $^*OOH$ species in oxidations involving kinetically-relevant O_2 activation. These intermediates have also been proposed to account for the ability of O_2/H_2O mixtures to act as reactants in alkene epoxidation on Au-based catalysts.

Published by Elsevier Inc.

1. Introduction

The catalytic oxidation of CO has been extensively used to probe mechanisms and site requirements in heterogeneous catalysis and to remove CO from combustion effluent and H_2-containing streams [1–3]. Au-based materials catalyze CO oxidation at sub-ambient temperatures when present as small Au clusters (<5 nm) dispersed on oxide supports (TiO_2, Fe_2O_3, Al_2O_3, etc.) [4–8]. The high reactivity of small Au clusters in CO oxidation catalysis has been variously attributed to the following: (i) low-coordination Au surface atoms, isolated Au atoms, or cationic Au species; (ii) electron transfer from the support to Au clusters; or (iii) supports that become active when placed in atomic contact with Au clusters [1]. The importance and relative contributions of these effects are controversial, and the specific evidence for each proposal remains equivocal and often contradictory.

Large differences in measured rates (>10-fold), in the observed effects of reactant and H_2O concentrations on such rates (kinetic order ranges of 0.02–1.01 and 0.07–0.46 for CO and O_2, respectively), and in deactivation rates have been reported on Au catalysts with similar cluster size, Au content, support material, and synthetic provenance [1,9]. The absence of consensus about these catalyst properties reflects, at least in part, the presence of adventitious H_2O at levels difficult to detect but consequential for catalysis. Previous studies have concluded that H_2O promotes [5,10,11], inhibits [12], or does not affect [13] CO oxidation catalysis. The most extensive studies [10,14] included Au clusters deposited on different supports (TiO_2, Al_2O_3, and SiO_2) and concluded that H_2O impurities in CO/O_2 reactants strongly increase CO oxidation rates, even at trace concentrations (0.1–1 ppm), which are undetectable by conventional analytical methods, and to very different extents on the various supports [14]. These H_2O effects have been attributed to the promotion of O_2 adsorption and/or dissociation, decomposition of unreactive carbonate deposits, and assistance in reducing inactive Au cations to Au^0 by CO [7,11,14–17], but their respective contributions remain the subject of persistent speculation and active debate. Recent reports also show that increasing concentrations of hydroxyl groups favor CO oxidation rates, either in alkaline aqueous phase using Au/TiO_2 and Au/C catalysts [18] or in the gas phase with Au/SiO_2 catalysts doped with NaOH [19].

Every plausible sequence of CO oxidation elementary steps and active sites has already been proposed, based on direct or indirect evidence, without even a modicum of consensus and with the implication of structures ranging from cationic or metallic Au species in some cases, but not others, in chemical or physical synergy

* Corresponding author. Fax: +1 510 642 4778.
E-mail address: iglesia@berkeley.edu (E. Iglesia).
[1] Present address: Institute of Catalysis and Petrochemistry (CSIC), C Marie Curie 2, 28049 Madrid, Spain.
[2] Present address: Chevron Corporation, Richmond, CA 94802, United States.

0021-9517/$ - see front matter Published by Elsevier Inc.
doi:10.1016/j.jcat.2011.09.015

with reducible or non-reducible supports, and with H_2O acting as a promoter, participant, inhibitor, or spectator species [1,5,16,20–23]. The only complete sequence of plausible elementary steps supported by the comparison with rigorous rate data, in our assessment, involves parallel competitive and non-competitive adsorption of CO and O_2 and their reactions in kinetically-relevant steps [24–26]; this mechanistic proposal did not consider what is currently accepted as a critical and perhaps even essential role of H_2O in mediating CO oxidation catalysis at near-ambient temperature.

We provide here kinetic and isotopic evidence for a sequence of elementary steps for CO oxidation on stable Au catalysts with added H_2O, present as a co-catalyst essential for stable turnover rates. These steps are mediated by hydroperoxy species (*OOH), which may form on Au surfaces [27], and which account for the co-catalytic effect of H_2O on CO oxidation rates and on catalyst stability and for the ability of these materials to catalyze propene epoxidation with H_2O/O_2 mixtures [28]. These kinetic data were obtained under conditions of strict kinetic control and without detectable deactivation in the presence of H_2O as an essential component; the data and their mechanistic interpretation aim to resolve long-standing controversies that reflect, at least in part, the instability and mechanistic promiscuity imposed by uncontrolled and undetected concentrations of adventitious H_2O in catalytic solids and reactant streams.

2. Experimental methods

2.1. Catalyst preparation and characterization

Al_2O_3-supported Au clusters (denoted here as Au/Al_2O_3) were prepared by the deposition–precipitation (DP) methods [5,20]. Tetrachloroauric acid hydrate (0.24 g, $HAuCl_4{\cdot}xH_2O$, 99.999%, Aldrich) was dissolved in doubly-distilled deionized H_2O (80 cm^3) at 353 K. γ-Al_2O_3 (5 g, Alcoa) was treated in flowing dry air (1.67 $cm^3\ s^{-1}\ g^{-1}$, UHP grade, Praxair) at 923 K for 5 h, and then dispersed in doubly-distilled deionized H_2O (120 cm^3) at 353 K. Au was deposited onto γ-Al_2O_3 surface at 353 K and a pH of 7 (adjusted with 0.5 M NaOH, >98%, Fluka) by stirring for 1 h. The resulting solids were rinsed and washed with doubly-distilled deionized H_2O (323 K) and dried at ambient temperature for 24 h. Samples were stored away from light without further treatment. The Au content was measured by inductively-coupled plasma emission spectroscopy (0.61% wt.; Galbraith Laboratories, Inc.). The mean diameter of these Au clusters (3.5 ± 1.2 nm) was determined by high-resolution transmission electron microscopy (TEM) and reported elsewhere [29]. Mean Au diameters (d_{Au}) were calculated using $d_{Au} = \sum n_i d_i^3 / \sum n_i d_i^2$, where d_i is the diameter measured from TEM images, and n_i is the number of Au clusters of diameter d_i. The pore size distribution was measured by N_2 adsorption–desorption at 77 K using a Micromeritics ASAP 2000 apparatus. Pore size distributions were obtained from these adsorption data using the Barrett–Joyner–Halenda (BJH) equation [30].

Three different portions of the Au/Al_2O_3 solids were treated in O_2/He (25 vol.%, 25 $cm^3\ g^{-1}\ s^{-1}$) by increasing the temperature from ambient to 873, 950, or 1023 K at 0.17 K s^{-1} and holding at each temperature for 2 h. These samples are denoted as treated catalysts, Au/Al_2O_3-X, where X represents the treatment temperature (X = 873, 950, or 1023), and the Au/Al_2O_3 solid dried at ambient temperature is named as untreated Au/Al_2O_3.

Two reference Au catalysts (1.56% wt. Au/TiO_2 and 4.44% wt. Au/Fe_2O_3, prepared by deposition–precipitation and co-precipitation, respectively) were provided by the World Gold Council (WGC). These two samples were used to examine the effects of support on CO oxidation rates and on the kinetic dependence of measured rates on reactant pressure in the presence and in the absence of co-fed H_2O; these materials were also used to evaluate CO oxidation pathways operating with Au clusters deposited on reducible and non-reducible metal oxide supports. The mean Au cluster size (d_{Au}) derived from TEM images are 3.3 ± 0.7 and 3.6 ± 0.7 nm for Au/TiO_2 and Au/Fe_2O_3, respectively.

A Pt/Al_2O_3 catalyst (2.03% wt., Pt clusters of 1.3 nm) was also used in reactions of $CO–O_2$ and $CO/O_2/H_2O$ mixtures to probe any effects of H_2O on CO oxidation rates on Pt clusters. The synthesis and characterization protocols used for this Pt catalyst have been reported elsewhere [31].

2.2. Steady-state CO oxidation rate measurements

CO oxidation rates were measured in a tubular packed-bed reactor with plug-flow hydrodynamics. Typically, catalysts (25–30 mg, 0.250–0.425 mm pellet size) were diluted with quartz granules (~1 g; washed with 1 M HNO_3 at 298 K for 2 h and then treated in ambient air at 1023 K for 5 h). Samples were treated in flowing pure H_2 (28 $cm^3\ s^{-1}\ g^{-1}$, 99.999%, Praxair) at 373 K (heating rate of 0.167 K s^{-1}) for 0.5 h and in H_2O/H_2 (28 $cm^3\ s^{-1}\ g^{-1}$, 1 vol.% H_2O) at 373 K for 0.5 h, using a previously reported procedure that forms stable Au metal clusters [32]. The catalyst was brought to the reaction temperature (282–303 K) in flowing He (99.999%, Praxair). Gas reactants (10 vol.% CO in He, 25 vol.% O_2 in He, UHP grade, <10 ppm H_2O, Praxair) were metered by electronic controllers, and H_2O (doubly-distilled and deionized) was introduced into heated transfer lines using a syringe pump (Cole Parmer 74900 Series). Helium was used as balance. CO, O_2, and He streams were further purified with moisture traps (Matheson Tri-Gas). Reactants and products concentrations were measured by gas chromatography (Agilent 6890 GC) using a Porapak Q packed column (80–100 mesh, 1.82 m × 3.18 mm) connected to a thermal conductivity detector (TCD). All transfer lines were heated to 400–415 K to prevent H_2O condensation. No reaction products were detected in the effluent when reactors contained only quartz diluent or Al_2O_3 supports. CO conversions were kept well below 10% in most experiments (and below 15% in cases) by changing residence times while keeping CO, O_2, and H_2O concentrations at constant values. These low conversions ensure the differential nature of measured rates and avoid their rigorous but more cumbersome interpretation in terms of integral equations.

Propene epoxidation rates using O_2/H_2O mixtures were measured on Au/TiO_2, while HCOOH dehydrogenation and water–gas shift reactions were performed with all Au/Al_2O_3 samples. Gas reactants (C_3H_6, 25 vol.% O_2 in He, 10 vol.% CO in He, UHP grade, Praxair) were metered by electronic controllers, and liquids HCOOH or H_2O (doubly-distilled deionized) were introduced using a syringe pump. Reactants and products concentrations were measured with a mass spectrometer (Inficon Transpector) and a gas chromatograph (Hewlett–Packard 5890) equipped with a Porapak Q packed column (80–100 mesh, 1.82 m × 3.18 mm) connected to a thermal conductivity detector and a HP-1 capillary column (50 m × 0.32 mm × 1.05 μm) connected to a flame ionization detector (FID).

2.3. Isotopic exchange rates and kinetic isotope effects

Isotopic $^{16}O_2/^{18}O_2$ and $^{16}O_2/H_2{}^{18}O$ exchange rates were measured on Au/Al_2O_3 using a glass recirculating flow reactor [33]. Samples were treated as described above, and the recirculating and reactor volumes (550 cm^3 total) were evacuated with mechanical and diffusion pumps before introducing reactants as vapors ($^{16}O_2$, 99.999%, Praxair; $^{18}O_2$, 99%, Isotec; $H_2{}^{18}O$, 99 at.% ^{18}O, Sigma–Aldrich). Chemical and isotopic compositions were measured by direct sampling into a gas chromatograph (Hewlett–Packard

5890) equipped with a thermal conductivity detector and an electron-impact mass selective detector (Hewlett–Packard 5972). D_2O (99.9% D, Cambridge Isotope Laboratories, Inc.) was used to measure H_2O/D_2O kinetic isotope effects (KIE) during CO oxidation using the tubular plug-flow reactor described in the previous section.

3. Results and discussion

3.1. Effects of H_2O on CO oxidation rates and catalyst stability

Fig. 1 shows CO oxidation rates at 288 K on untreated Au/Al_2O_3 with and without added H_2O. H_2O strongly influenced CO oxidation turnover rates (per surface gold atom, Au_s; from mean TEM cluster sizes, 3.5 ± 1.2 nm), as also shown previously [10]. CO oxidation rates did not vary (2.55 ± 0.10 mol s^{-1} g-at Au_s^{-1}) with time-on-stream for the duration of this experiment (~25 ks; Fig. 1) or of similar experiments on all other catalysts reported here when H_2O (0.5 kPa) was present in CO/O_2 reactant mixtures (5 kPa CO; 2 kPa O_2). These conditions led to stable CO oxidation rates at levels that rank among the highest reported on Au-based catalysts [9]. In contrast, CO conversion rates decreased rapidly to ~ 0.08 mol s^{-1} g-at Au_s^{-1} (first-order deactivation rate constant, k_d, 0.76 ks^{-1} initially and 0.21 ks^{-1} after 3 ks on stream) when H_2O was removed from the reactant stream and the concentration of residual H_2O decreased with time. The initial CO oxidation rates were fully recovered upon reintroduction of H_2O (0.5 kPa) into the reactant mixture (Fig. 1), indicating that the effects of H_2O were reversible and that the absence of H_2O did not cause sintering or other irreversible structural changes.

The effects of H_2O concentration on steady-state CO oxidation turnover rates are shown in Fig. 2. Turnover rates initially increased with H_2O pressure at low concentrations (<0.2 kPa) and reached a maximum value at ~0.5 kPa H_2O; higher H_2O concentrations inhibited CO oxidation reactions. These positive and reversible effects of H_2O are consistent with some previous studies [16,20,34]; the inhibition observed at higher pressures may account for persistent contradictory reports about the specific effects of H_2O on Au-catalyzed CO oxidation [12]. The promotion effects of H_2O are not caused by parallel water–gas shift (WGS) reactions ($CO + H_2O \rightarrow CO_2 + H_2$), because CO_2 was not formed from CO/H_2O mixtures (5 kPa CO; 2 kPa H_2O) on this Au/Al_2O_3 catalyst, even at higher temperatures (~350 K).

Positive H_2O effects have been previously attributed to the decomposition of carbonates formed on Au active sites during CO oxidation in the absence of H_2O [16,34]. In contrast, other studies implicate, without specific experimental evidence, a role of H_2O in elementary steps required for O_2 activation, possibly via the formation of activated oxygen species that react rapidly with CO to form intermediates that ultimately decompose to CO_2 [14,35]. The possible involvement of H_2O in the kinetically-relevant steps in CO oxidation catalytic sequences is examined next by comparing CO oxidation turnover rates (288 K, 5 kPa CO, 2 kPa O_2) measured on Au/Al_2O_3 using H_2O or D_2O (0.5 kPa) as additives. As we show later (Section 3.4), the small measured H_2O/D_2O isotope effects indicate that O–H(D) bonds are not cleaved in kinetically-relevant steps in the CO oxidation catalytic sequence.

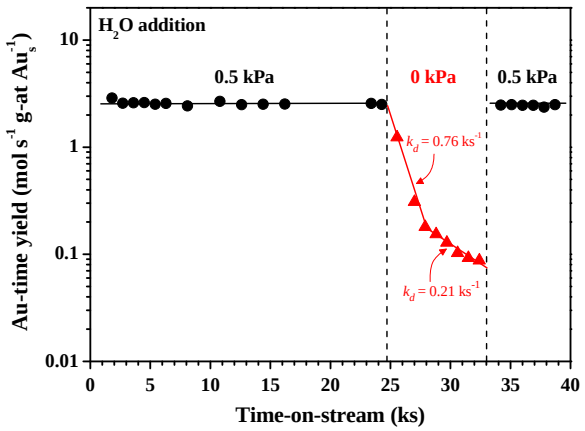

Fig. 1. H_2O effect in CO oxidation turnover rates measured with the untreated Au/Al_2O_3 (0.61% wt., 288 K, 5 kPa CO, 2 kPa O_2). Symbols: (●) 0.5 kPa H_2O; (▲) 0 kPa H_2O.

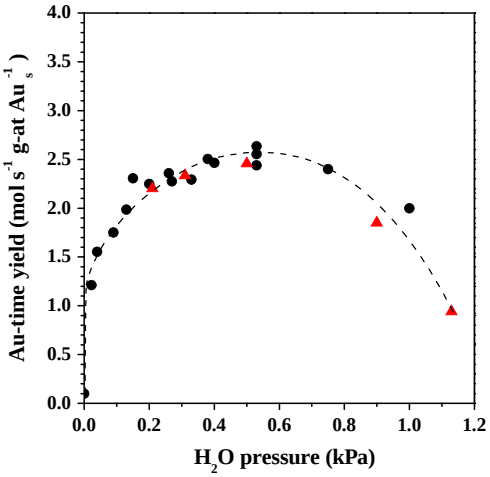

Fig. 2. Influence of H_2O pressure (0.03–7.15 kPa) on CO oxidation turnover rates measured with the untreated Au/Al_2O_3 (0.61% wt., 288 K, 5 kPa CO, 2 kPa O_2). Pellet size: 0.125–0.250 mm (●); 0.250–0.425 mm (▲).

Previous studies have proposed that H_2O inhibition effects (>0.5 kPa) reflect competitive adsorption by H_2O-derived intermediates [10,36]. It is also possible that H_2O condensation within catalyst mesopores imposes diffusional corruptions of chemical reaction rates by decreasing intrapellet CO or O_2 concentrations and thus the kinetic driving force for CO oxidation at active sites. We find, however, that CO oxidation turnover rates did not depend on pellet size (0.125–0.250 and 0.250–0.425 mm diameter; Fig. 2); thus, even if condensation occurred, the presence of H_2O within alumina pores did not impose transport barriers, which would have caused smaller rates on the larger pellets. Moreover, the pore size distribution of the Al_2O_3 used in this study did not lead to detectable pore filling below ~1.5 kPa H_2O at reaction temperatures (Supplementary Content). We conclude that the H_2O inhibition observed above ~0.5 kPa (Fig. 2) reflects competitive adsorption of H_2O-derived adsorbed species with reactive intermediates derived from CO or O_2 on Au clusters and arise from chemical origins instead of any transport corruptions.

Thermal treatments of Au/Al_2O_3 in 25 vol.% O_2/He at temperatures up to 1023 K did not lead to detectable changes in Au cluster size (transmission electron microscopy, TEM; Supplementary Content) or in CO oxidation rates in the presence of H_2O (288 K, 5 kPa - CO, 2 kPa O_2, 0.5 kPa H_2O; Table 1), indicating that Au clusters on Al_2O_3 resist sintering even at these high temperatures and that the deactivation of Au-based catalysts reported during CO oxidation in the absence of H_2O at near-ambient temperatures cannot reflect cluster growth. These data also show that CO oxidation occurs on the Au clusters visible in transmission electron micrographs. In contrast, the rates of HCOOH dehydrogenation (353 K, 2 kPa HCOOH) and water–gas shift (523 K, 5 kPa CO, 2 kPa H_2O) decreased markedly with increasing treatment temperature, apparently as a result of the disappearance of smaller Au structures

Table 1
Influence of Au/Al_2O_3 treatment temperature (O_2/He, 2 h) on Au clusters size obtained by TEM and on rates for CO oxidation, HCOOH dehydrogenation, and water–gas shift reactions.

Catalyst	Treatment temp. (K)	Mean Au size (nm)	Rate (mol h^{-1} g-at Au^{-1})		
			CO–O_2–H_2O[a]	HCOOH[b]	CO–H_2O[c]
Au/Al_2O_3	–	3.5 ± 1.2	2589	477	110
Au/Al_2O_3-873	873	4.0 ± 1.0	2827	201	74
Au/Al_2O_3-950	950	4.0 ± 1.1	2535	85	57
Au/Al_2O_3-1023	1023	4.3 ± 1.2	2610	40	30

[a] 288 K, 5 kPa CO, 2 kPa O_2, 0.5 kPa H_2O.
[b] 353 K, 2 kPa HCOOH.
[c] 523 K, 5 kPa CO, 2 kPa O_2.

undetectable at the resolution of these transmission electron micrographs (Table 1) [29].

3.2. Kinetic dependence of CO oxidation rates on reactants pressure and temperature

The stable CO oxidation turnover rates observed in the presence of H_2O allowed accurate and reproducible kinetic measurements over a wide range of CO, O_2, and H_2O pressures. Next, we report the kinetic effects of CO and O_2 pressures on CO oxidation turnover rates on Au/Al_2O_3 (0.5 kPa H_2O; Fig. 3). CO oxidation turnover rates increased with increasing CO (0.80–8.25 kPa) and O_2 (0.25–7.15 kPa) pressures, with empirical fractional orders of 0.24 ± 0.02 and 0.60 ± 0.02, respectively. Au/Al_2O_3 treated in O_2/He at various higher temperatures (873–1023 K) gave similar kinetic effects of CO (0.15–0.25 order) and O_2 (0.55–0.60 order) (288 K, 1–6 kPa CO, 0.5–6 kPa O_2, 0.5 kPa H_2O) and they also requires co-fed H_2O for high and stable CO oxidation turnover rates (Supplementary Content). These fractional reaction orders, taken at face value, cannot be reconciled with any sequence of elementary steps. Yet, it is in such a manner that kinetic data on Au catalysts have been invariably reported; we do so here, only momentarily, to show that these fractional orders lie within the broad range reported in previous studies using nominally anhydrous CO/O_2 mixtures (0.1–0.5 and 0.3–0.6 for CO and O_2, respectively [1,7,9,24,37,38]). The positive orders in both CO and O_2 indicate that either both CO and O_2 are present below saturation coverages on Au surfaces during CO oxidation or that they adsorb non-competitively on distinct active sites.

CO oxidation turnover rates (5 kPa CO, 2 kPa O_2, 0.5 kPa H_2O) on Au/Al_2O_3 catalysts increased with temperature (282–303 K) in a manner consistent with an apparent activation energy of 36 ± 3 kJ mol^{-1} (Fig. 4); these values lie within the range reported by other authors (22–40 kJ mol^{-1}) on Au/Al_2O_3 (1.2–5.6 nm Au clusters) in the presence of H_2O (40 ppm) or H_2 (0.25–75 kPa) at 303–453 K [14,34,39]. However, in the absence of H_2O, other authors found lower CO oxidation activation energies (12 ± 1 kJ mol^{-1}, 295–373 K) with Au/Al_2O_3 (1.2 nm Au) [34]. Moreover, erratic and large differences in activation energies, ranging from 8 to 75 kJ mol^{-1}, have been reported in the literature for nominally anhydrous CO/O_2 reactions on Au clusters deposited on reducible and non-reducible supports (TiO_2, Fe_2O_3, CeO_2, SiO_2, etc.).

3.3. CO–O_2 reaction pathways on Au/Al_2O_3 in the presence of H_2O

Scheme 1 depicts a sequence of elementary steps for low-temperature CO oxidation reaction consistent with the kinetic data discussed in Section 3.2. Steps 1, 2, and 3 represent quasi-equilibrated non-dissociative adsorption steps for all species in the reactant stream (CO, O_2, and H_2O). O_2 adsorption is assumed to be molecular and reversible. Irreversible O_2 adsorption (whether molecular or dissociative) would lead to CO oxidation rates proportional to O_2 pressures, in contradiction with our kinetic data and with most previous reports [1]. Reversible O_2 adsorption and subsequent reactions with the CO^* species present as most abundant reaction intermediates (MARI) would also lead to first-order O_2 kinetics,

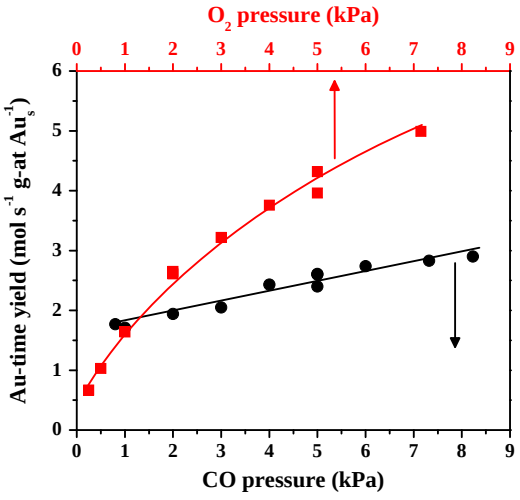

Fig. 3. Kinetic dependence of CO oxidation turnover rates on CO pressure (0.80–8.25 kPa CO, 2 kPa O_2, 0.5 kPa H_2O) and O_2 pressure (0.25–7.15 kPa O_2, 5 kPa CO, 0.5 kPa H_2O) measured with the untreated Au/Al_2O_3 (0.61% wt., 288 K).

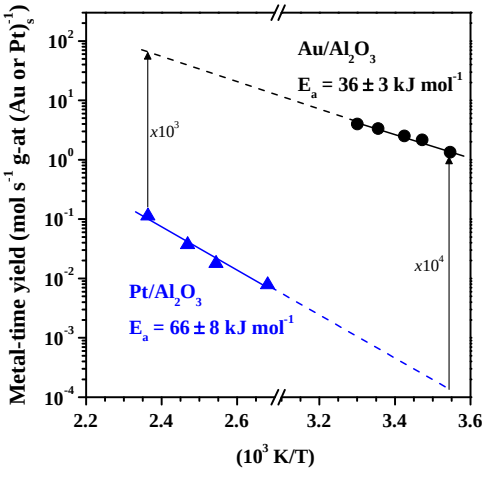

Fig. 4. Arrhenius plots for the CO oxidation (5 kPa CO; 2 kPa O_2; 0.5 kPa H_2O) measured with the untreated Au/Al_2O_3 (●, 0.61% wt., 3.5 nm Au, 282–303 K) and Pt/Al_2O_3 (▲, 2.03% wt., 1.3 nm Pt, 373–423 K). Rates with Pt/Al_2O_3 were determined at 1 kPa CO and 10 kPa O_2 and recalculated according to previously reported and well-established CO and O_2 pressures effects on measured kinetics (+1 and −1 reaction orders for O_2 and CO pressure, respectively) [31].

1. $CO + * \rightleftharpoons CO*$ K_1
2. $O_2 + * \rightleftharpoons O_2*$ K_2
3. $H_2O + * \rightleftharpoons H_2O*$ K_3
4. $O_2* + H_2O* \rightleftharpoons *OOH + *OH$ K_4
5. $*OOH + CO* \longrightarrow *OH + CO_2 + *$ k_5
6. $*OH + *OH \longrightarrow H_2O* + O*$ k_6
7. $CO* + O* \longrightarrow CO_2 + 2*$ k_7

Scheme 1. CO oxidation pathways on Au/Al_2O_3 at low temperatures in the presence of co-fed H_2O (* denotes a vacant active site and X* the various adsorbed species).

suggesting that alternate steps must be involved in the activation of O_2^* species. Step 4 represents the formation of hydroperoxy species (*OOH) via proton transfer from water to O_2^*, in a step assumed to be fast and quasi-equilibrated based on the small measured H_2O/D_2O kinetic isotope effects (Section 3.4). In this sequence, O–O bond activation is assisted by H_2O, in a step that avoids the difficult dissociation of O_2 on Au surfaces; this step forms *OOH species that then react with CO* to form CO_2 (step 5). Catalytic turnovers are completed via the recombination of *OH species (step 6) to re-form the H_2O molecule used to activate O_2^* (which therefore acts as a co-catalyst instead of a stoichiometric reactant) and an O* atom; the latter is ultimately removed via the reaction with CO* to form another CO_2 molecule (step 7), a step that exhibits a low activation barrier (~24 kJ mol^{-1}) according to previous theoretical estimates on Au(211) and Au(221) model surfaces [40]. *OH recombination to HOOH* (*OH + *OH → HOOH* + *) is not considered as a plausible alternate path to the proposed H_2O^* + O* reaction (E_a = 17–25 kJ mol^{-1} [41,42]) based on DFT estimates on Au(111) showing a much higher activation energy barrier (157 kJ mol^{-1}) [43]).

The assumption of pseudo-steady-state [44] for all adsorbed species and of quasi-equilibrium for steps 1–4 in Scheme 1 leads to the following CO oxidation rate equation, the full algebraic derivation of which is included in Appendix A:

$$r = \frac{\alpha\,(P_{CO}\,P_{O_2}\,P_{H_2O})^{2/3}}{\left[1 + K_1P_{CO} + K_2P_{O_2} + K_3P_{H_2O} + (\beta+\gamma)\frac{(P_{O_2}P_{H_2O})^{2/3}}{P_{CO}^{1/3}} + \delta\,(P_{CO}P_{O_2}P_{H_2O})^{1/3}\right]^2} \quad (1)$$

(1)

Each term in the denominator of this equation represents the concentration of the indicated adsorbed intermediate relative to the concentration of vacant sites on Au cluster surfaces. In Eq. (1), K_1, K_2, and K_3 are the equilibrium constants for molecular CO, O_2, and H_2O adsorption, respectively, and α, β, γ, and δ are given by the combinations of rate and equilibrium constants for elementary steps

$$\alpha = 3/2(K_1K_2K_3K_4K_5)^{2/3}(2K_6)^{1/3} \quad (2)$$

$$\beta = (K_2K_3K_4)^{2/3}(2K_6)^{1/3}(K_1K_5)^{-1/3} \quad (3)$$

$$\gamma = K_1^{-1/3}(K_2K_3K_4K_5)^{2/3}(K_6)^{1/3}(2)^{-2/3}(K_7^{-1}) \quad (4)$$

$$\delta = (K_2K_3K_4K_5)^{1/3}(2K_6)^{1/3} \quad (5)$$

The values of the kinetic parameters β, γ, and δ derived from the nonlinear regression analysis of measured CO oxidation rates make the terms in the denominator of Eq. (1) containing these constants (relative surface coverage of O*, *OH, and *OOH) to be much smaller than the others (vacant sites, CO*, O_2^*, and H_2O^*; Supplementary Content) at the conditions of our experiments. Therefore, Eq. (1) becomes

$$r = \frac{\alpha(P_{CO}P_{O_2}P_{H_2O})^{2/3}}{[1 + K_1P_{CO} + K_2P_{O_2} + K_3P_{H_2O}]^2} \quad (6)$$

when assuming that *OOH, *OH, and O* are minority surface species present in much lower concentrations than vacant sites (*), CO*, O_2^*, and H_2O^*.

The parity plot in Fig. 5 shows that Eq. (6) accurately describes the measured effects of reactants pressures (0.80–8.25 kPa CO; 0.25–7.15 kPa O_2; 0.03–1.15 kPa H_2O) on CO oxidation turnover rates on Au/Al_2O_3. We did not find other assumptions about most abundant surface species or about quasi-equilibrated steps consistent with these measured rates. Alternate $CO/O_2/H_2O$ reaction pathways were also considered (Supplementary Content), but rigorous kinetic and isotopic (shown later) analyses demonstrated that none of them was able to successfully predict measured rate data. The kinetic parameters derived from the nonlinear regression analysis of measured CO oxidation rates with Au/Al_2O_3 are shown in Table 2. The H_2O adsorption equilibrium constant (3.1 ± 0.6 kPa^{-1}) is larger than for CO and O_2 (0.18 ± 0.05 and 0.06 ± 0.02 kPa^{-1}, respectively); CO is indeed expected to bind more strongly than O_2, based on first-principle density functional theory (DFT) with generalized gradient approximation (GGA) calculations on $Au/Al_2O_3(100)$ and Au_8–Au_{30} model systems, which gave CO adsorption energies (90–100 kJ mol^{-1}) much greater than for O_2 (5–70 kJ mol^{-1}) [41,45–47]. The measured H_2O adsorption constant (K_3) is, however, somewhat larger than the expected from

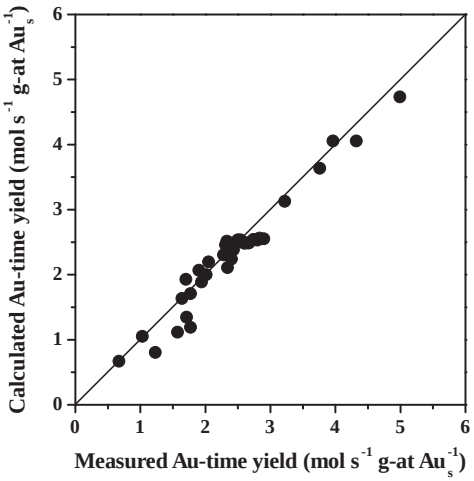

Fig. 5. Parity plot for measured (0.61% wt. Au/Al_2O_3; 288 K; 0.80–8.25 kPa CO; 0.25–7.15 kPa O_2; 0.03–1.15 kPa H_2O) and calculated (from Eq. (6)) CO oxidation turnover rates.

Table 2
Kinetic parameters for the CO oxidation model in the presence of H_2O (Scheme 1) obtained from nonlinear fitting to Eq. (6) of kinetic data measured with Au/Al_2O_3, Au/TiO_2, and Au/Fe_2O_3 catalysts.

Kinetic parameter	Au/Al_2O_3	Au/TiO_2	Au/Fe_2O_3
α (s^{-1} kPa^{-2})	11.0 ± 3.4	12.3 ± 3.4	1.3 ± 0.4
K_1 (kPa^{-1})	0.18 ± 0.05	0.24 ± 0.09	0.18 ± 0.07
K_2 (kPa^{-1})	0.06 ± 0.02	0.05 ± 0.02	0.16 ± 0.06
K_3 (kPa^{-1})	3.1 ± 0.6	3.4 ± 0.9	1.1 ± 0.5

$\alpha = 3/2(K_1K_2K_3K_4K_5)^{2/3}(2K_6)^{1/3}$.

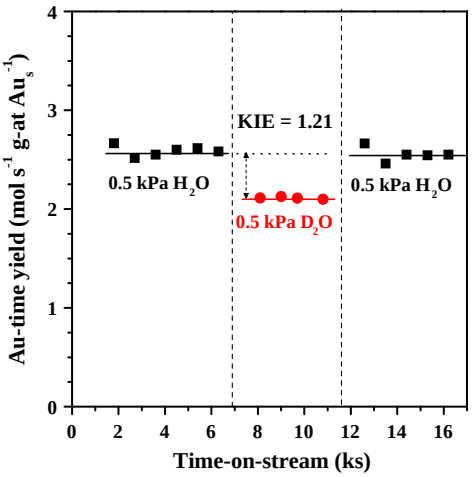

Fig. 6. H_2O/D_2O isotope effects on CO oxidation turnover rates measured with Au/Al_2O_3 (0.61% wt., 288 K; 5 kPa CO; 2 kPa O_2; 0.5 kPa H_2O (■) or D_2O (●)).

the Au–H_2O interaction energies reported from previous theoretical treatments on model Au_8–Au_{30}, $Au/Al_2O_3(100)$, and $Au/TiO_2(110)$ surfaces (30–100 kJ mol^{-1}) [42,48].

3.4. H_2O/D_2O isotope effects and isotopic exchange measurements

H_2O/D_2O isotope effects were used to probe the potential involvement of H_2O and of O–H bond activation in kinetically-relevant steps in the context of the CO oxidation catalytic sequence depicted in Scheme 1. CO oxidation turnover rates (288 K, 5 kPa CO, 2 kPa O_2) were measured on untreated Au/Al_2O_3 by adding H_2O or D_2O (0.5 kPa) to CO/O_2 reactant streams (Fig. 6). The small measured H_2O/D_2O isotope effects ($rH_2O/rD_2O = 1.21$; Fig. 6) are consistent with previous studies that report H_2O/D_2O isotope effects near unity on Au/Al_2O_3 (295 K, 1 kPa CO, 0.5 kPa O_2, 1.5 kPa $H_2O(D_2O)$) [16]. These data lead us to conclude that O–H (or O–D) bonds are not cleaved in kinetically-relevant steps, which would have shown large normal isotope effects at these low temperatures (288 K). These small normal H_2O/D_2O isotope effects reflect their probable thermodynamic origins stemming from quasi-equilibrated H_2O dissociation steps that occur before kinetically-relevant steps in CO oxidation catalytic sequences.

Next, we probe O_2 chemisorption steps on Au/Al_2O_3 by measuring the rate of formation of $^{16}O^{18}O$ isotopologues from equimolecular $^{16}O_2/^{18}O_2$ mixtures (5 kPa) at 300 K in the absence of CO and H_2O. Quasi-equilibrated dissociation would form binomial isotopologue distributions (50% $^{16}O^{18}O$), while molecular adsorption steps would not form mixed $^{16}O^{18}O$ isotopes. The rate of $^{16}O^{18}O$ formation (300 K, 5 kPa $^{16}O_2$, 5 kPa $^{18}O_2$) was ~50 times smaller than CO oxidation rates (288 K, 5 kPa CO, 2 kPa O_2, 0.5 kPa H_2O) even at higher temperatures and O_2 pressures than those used in CO oxidation catalysis (Fig. 7a); these findings are consistent with previous studies that reported no detectable $^{16}O^{18}O$ formation during $^{16}O_2/^{18}O_2$ isotopic exchange at similar pressures on Au/TiO_2 (353 K) and Au/Fe_2O_3 (298 K) [13,49] and show that O_2 adsorbs molecularly ($O_2 + * \leftrightarrow O_2^*$) on Au clusters.

The rate of isotopic exchange between $^{16}O_2$ (5 kPa) and $H_2{}^{18}O$ (0.5 kPa) was also measured on Au/Al_2O_3 at 300 K in the absence of CO. The formation of $^{16}O^{18}O$, $^{18}O_2$, or $H_2{}^{16}O$ molecules was not detected (Fig. 7b). The absence of isotopic exchange between O_2 and H_2O reflects the non-dissociative nature of O_2 adsorption on Au, as also inferred from the absence of $^{16}O_2/^{18}O_2$ exchange. We note that steps 2–4 in the catalytic sequence do not lead to the cleavage of O–O bonds, which instead occurs in latter steps via reactions with CO* in CO oxidation and with propene in propene epoxidation on Au catalysts [28]; as a result, the equilibrated nature of these O_2 adsorption and reaction steps cannot cause isotopic oxygen exchange.

3.5. Support effects on CO oxidation rates with Au-based catalysts

The identity of the support has been often implicated as an essential second function in the reactivity of Au clusters in CO oxidation [1,5,6,24,50], either via its participation in O_2 activation or because of its ability to stabilize small Au clusters. Reducible oxides (e.g., TiO_2, Fe_2O_3) have been reported to catalyze CO oxidation at higher rates than refractory oxides (e.g., Al_2O_3, SiO_2), a finding attributed to the requirement for O_2 activation on periphery sites located at Au-support interfaces [6,51]. The data used to reach these conclusions were obtained under nominally anhydrous conditions, but possibly in the presence of catalytically-consequential levels of H_2O, derived, at least in part, from H_2O adsorbed on supports and at concentrations that decrease with time as H_2O is depleted by desorption from these supports. These processes may have led, in turn, to the decrease in rates with time often interpreted as catalyst deactivation during CO oxidation on Au-based catalysts.

Fig. 8 and Table 3 compare turnover rates on Au clusters of similar size dispersed on reducible (TiO_2 and Fe_2O_3, 3.3 ± 0.7 and 3.6 ± 0.7 nm Au clusters, respectively) and non-reducible (Al_2O_3,

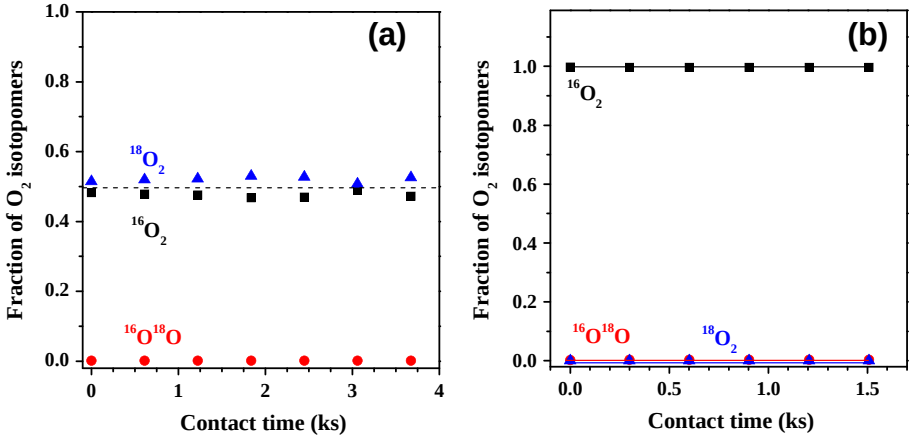

Fig. 7. Molar fraction of $^{16}O_2$ (■), $^{16}O^{18}O$ (●), and $^{18}O_2$ (▲) during contact at 300 K of equimolar $^{16}O_2/^{18}O_2$ (a, 5 kPa) or $^{16}O_2/H_2{}^{18}O$ (b, 5 kPa O_2, 0.5 kPa H_2O) on Au/Al_2O_3 (0.61% wt.; untreated).

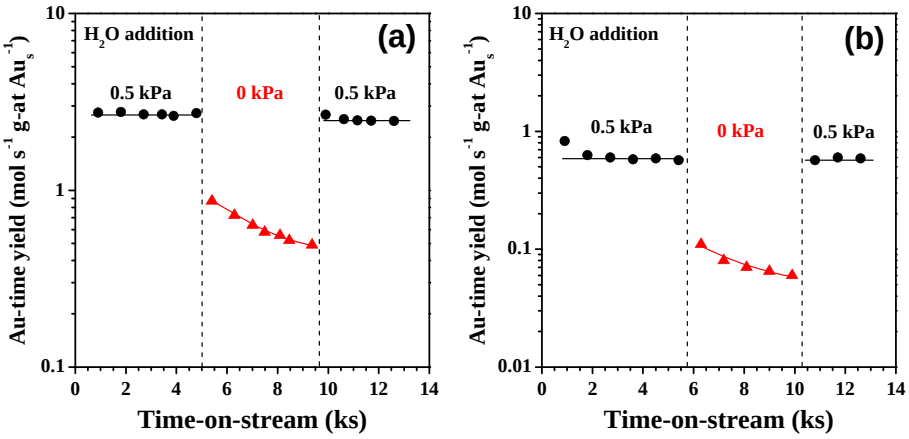

Fig. 8. H_2O effect on CO oxidation turnover rates (288 K, 5 kPa CO, 2 kPa O_2) measured with Au/TiO_2 (a) and Au/Fe_2O_3 (b). Symbols: (●) 0.5 kPa H_2O; (▲) 0 kPa H_2O.

Table 3
Effect of H_2O addition (0.5 kPa) on CO oxidation turnover rates (288 K, 5 kPa CO, 2 kPa O_2) for Au clusters deposited onto Al_2O_3 (0.61% wt. Au), TiO_2 (1.56% wt. Au), and Fe_2O_3 (4.44% wt. Au).

	CO oxidation turnover rate (mol s^{-1} g-at Au_s^{-1})	
Added H_2O (kPa)	0	0.5
Au/Al_2O_3	0.08	2.55
Au/TiO_2	0.54	2.70
Au/Fe_2O_3	0.07	0.59

3.5 ± 1.2 nm Au clusters) oxides for CO/O_2 and $CO/O_2/H_2O$ reactants. As in the case of Au/Al_2O_3 catalysts, the addition of H_2O as a co-catalyst was essential for stable turnover rates on Au/TiO_2 and Au/Fe_2O_3. H_2O (0.5 kPa) increased CO oxidation rates on all catalysts, but to different extents, possibly because of the presence of support-dependent H_2O concentrations even for nominally anhydrous $CO–O_2$ reactants. Turnover rates with anhydrous $CO–O_2$ reactants (based on TEM mean cluster sizes) on Au/TiO_2 were significantly higher than on Au/Al_2O_3 (~7 times), in agreement with literature claims for the benefits of reducible oxide supports. $CO/O_2/H_2O$ mixtures, however, gave similar rates on Au/TiO_2 and Au/Al_2O_3 (2.70 and 2.55 mol s^{-1} g-at Au_s^{-1}, respectively) and somewhat smaller rates on Au/Fe_2O_3 (0.59 mol s^{-1} g-at Au_s^{-1}). The latter values appear to reflect the encapsulation of some TEM-visible Au clusters within Fe_2O_3 as a consequence of the co-precipitation methods used, which in contrast with the deposition–precipitation method used for TiO_2 and Al_2O_3 supports do not ensure the presence of Au clusters at accessible support surfaces.

We conclude from these data that supports influence CO oxidation turnover rates with anhydrous reactants, perhaps because they can contribute adsorbed H_2O as co-catalyst or as periphery sites that become essential for O_2 activation only under anhydrous conditions. These support effects and specifically the reducible nature of the support become much less consequential when H_2O mediates the required O_2 activation steps. The observed H_2O effects on CO oxidation rates with Au/TiO_2 and Au/Fe_2O_3 also suggest that the mechanistic pathways in Scheme 1 are also involved in CO oxidation reactions on reducible supports, as long as H_2O is present as a co-catalyst. These elementary steps occur on Au cluster surfaces without any significant requirement for a second function provided by either interfacial or support sites. This is also consistent with previous reports [14] showing similar CO oxidation activation energies on Au/TiO_2 and Au/Al_2O_3 (22 and 25 kJ mol^{-1}, respectively), which suggests a common reaction mechanism over these two catalysts.

The effects of CO and O_2 pressure on CO oxidation turnover rates on Au/TiO_2 and Au/Fe_2O_3 (Fig. 9; 288 K, 0.5 kPa H_2O) were

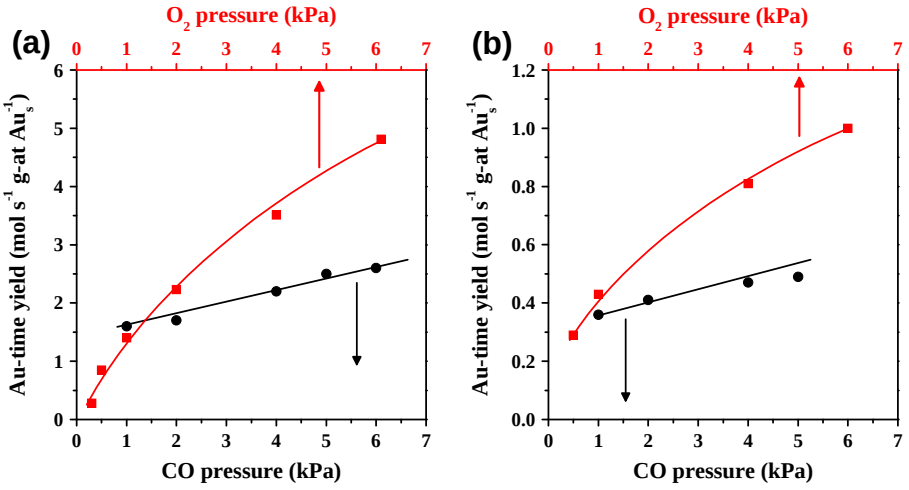

Fig. 9. Kinetic dependence of CO oxidation turnover rates on CO (●, 1–5 kPa CO, 2 kPa O_2, 0.5 kPa H_2O) and O_2 (■, 0.5–6 kPa O_2, 5 kPa CO, 0.5 kPa H_2O) pressures measured at 288 K with Au/TiO_2 (a) and Au/Fe_2O_3 (b).

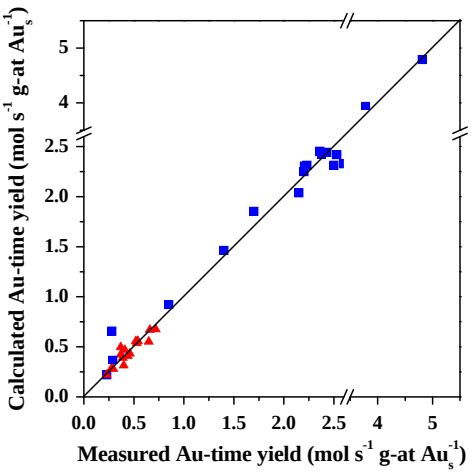

Fig. 10. Parity plot for measured (288 K; 1–6 kPa CO; 0.5–6 kPa O_2; 0.12–0.53 kPa H_2O) and calculated (from Eq. (6)) CO oxidation turnover rates with Au/TiO_2 (▪) and Au/Fe_2O_3 (▲).

similar to those measured on Au/Al_2O_3 (Fig. 3). Turnover rates increased with CO pressure (1–6 kPa, 0.29 ± 0.04, and 0.19 ± 0.02 orders on Au/TiO_2 and Au/Fe_2O_3, respectively) and O_2 pressure (0.5–6 kPa, 0.68 ± 0.01, and 0.49 ± 0.02 orders on Au/TiO_2 and Au/Fe_2O_3, respectively). The sequence of elementary steps in Scheme 1 therefore appears to be generally applicable to CO oxidation reactions with CO–O_2–H_2O reactants on Au clusters dispersed on all three supports. The rate equation derived from the steps in Scheme 1 (Eq. (6)) accurately described all rate data as a function of CO, O_2, and H_2O pressures on Au/TiO_2 and Au/Fe_2O_3. Fig. 10 shows the respective parity plots of measured and predicted turnover rates, and Table 1 lists the regressed kinetic parameters. As found on Au/Al_2O_3, H_2O adsorption equilibrium constants are larger than for CO and O_2 on Au/TiO_2 and Au/Fe_2O_3 (Table 2). The values of K_1, K_2, and K_3 are similar on all supports, consistent with the similar size of Au clusters and their exclusive involvement in mediating the elementary steps in Scheme 1.

3.6. Evidence for the presence and reactivity of hydroperoxy (*OOH) species on Au

The elementary steps for CO–O_2 reactions in the presence of H_2O (Scheme 1) and the assumptions made about their reversibility lead to a rate equation (Eq. (6)) consistent with measured rates on Au clusters dispersed on both reducible (TiO_2, Fe_2O_3) and non-reducible (Al_2O_3) supports. These steps and assumptions are also consistent with H_2O/D_2O isotope effects on CO oxidation rates and with the absence of isotopic exchange in $^{16}O_2/^{18}O_2$ and $^{18}O_2/H_2{}^{16}O_2$ mixtures. O_2 activation involves reactions of O_2^* and H_2O^* to form hydroperoxy species (*OOH) with intact O–O bonds, but weaker relative to those in O_2 molecules. These *OOH intermediates also account for the reactivity of small Au clusters in the formation of H_2O_2 from H_2–O_2 mixtures [52,53], which proceeds via *OOH intermediates, as shown from theoretical estimates [27], electronic and spin resonance spectra [54], and inelastic neutron scattering [55]. *OOH species also account for propylene epoxidation with H_2/O_2 mixtures on Au-based catalysts [56,57]. These *OOH species have been also proposed to account for the promotion of CO oxidation by H_2, without specific direct evidence [35,39,58]. The formation of H_2O_2 has been detected by UV–visible spectroscopy during CO oxidation on Au/TiO_2 and Au/C in aqueous alkaline media [18].

The formation of *OOH species from O_2/H_2O mixtures is also evident from the formation of propylene oxide from propene at near-ambient temperatures on Au/TiO_2 (Table 4, 350 K) [28], a finding later confirmed by propylene oxide synthesis from CO/O_2/propene mixtures in aqueous Au/TiO_2 and TS-1 suspensions [59]. These epoxidation reactions provide independent evidence for the formation of *OOH species from O_2–H_2O reactants and for their involvement in O_2 activation during CO oxidation reactions. These O_2 activation pathways occur on Au clusters surfaces without detectable involvement of the support and remove the need for support-mediated O_2 activation at the periphery of Au clusters as a requirement for CO oxidation catalysis. Theoretical calculations on Au_8 and Au_{30} clusters indicate that coadsorbed H_2O and O_2 form $O_2{\cdot}H_2O$ complexes via partial proton sharing or transfer with low activation barriers (17–25 kJ mol^{-1}) to form *OOH species [41,42]. *OOH species may be responsible for the well-established promotional effect of H_2 in CO/O_2 reaction on Au catalysts [1,34,39,60,61], as proposed previously for model Ru–Pt core shell nanoparticles from first-principles calculations consistent with atomic H* addition to O_2^* to form *OOH as the relevant pathway in the preferential oxidation of CO in H_2-rich streams [62].

Table 4
Effect of H_2O addition on initial (extrapolated to zero time-on-stream) propene epoxidation rates and selectivity (350 K, 4 kPa C_3H_6, 4 kPa O_2) with Au/TiO_2 (1.56% wt. Au, WGC). Table adapted from reference [28].

H_2O pressure (kPa)	Metal-time yield (mol h^{-1} g-at Au^{-1})	Selectivity (%, carbon based)	
		Propene oxide	Acetone
1	0.35	85.2	14.8
2	0.51	75.0	25.0
6	0.52	39.7	60.3
12	0.57	24.1	75.9

3.7. H_2O effects on CO oxidation turnovers catalyzed by supported Pt clusters

A catalytic effect of H_2O was also observed during CO oxidation on Pt clusters, the origins of which have not, to our knowledge, been examined in the extensive previous literature dealing with Pt-catalyzed CO oxidation catalysis [63,64]. Fig. 11a shows CO oxidation turnover rates on Pt/Al_2O_3 at 423 K (2.03% wt., 1.3 nm Pt clusters) with and without added H_2O. CO oxidation rates decreased from 0.28 to 0.08 mol s^{-1} g-at Pt_s^{-1} in ~1 ks when H_2O (0.5 kPa) was removed from the reactant mixture (1 kPa CO, 10 kPa O_2). Initial CO oxidation rates were fully recovered upon reintroduction of H_2O (0.5 kPa, Fig. 11a). The parallel formation of CO_2 via water–gas shift occurs at negligible rates ($< 10^{-3}$ mol s^{-1} g-at Pt_s^{-1}, Pt clusters of 0.9–1.7 nm) at these temperatures (423 K, 3 kPa CO, 10 kPa H_2O) [63,65]. The data in Fig. 11a suggest that H_2O also provides a more facile route for O_2 activation during CO oxidation on CO-covered Pt clusters. A recent study combining theory and experiment [31] showed that anhydrous CO oxidation on Pt occurs via CO*-assisted O_2 dissociation steps on surfaces nearly saturated by chemisorbed CO* intermediates, which hinder O_2 adsorption and subsequent activation. The presence of H_2O may act to decrease local CO* coverages and weaken inhibition effects by CO [64], but may also provide *OOH species as alternate O_2 activation routes with lower activation barriers and concomitantly higher CO oxidation turnover rates than the CO-assisted O_2 activation steps that limit CO oxidation with anhydrous CO/O_2 mixtures. Indeed, apparent activation energies decrease from 84 ± 6 kJ mol^{-1} (403–473 K, 1 kPa CO, 10 kPa O_2) [31] to 66 ± 8 kJ mol^{-1} (373–423 K, 1 kPa CO, 10 kPa O_2, 0.5 kPa H_2O, Fig. 11b) when H_2O was present in CO/O_2 reactants.

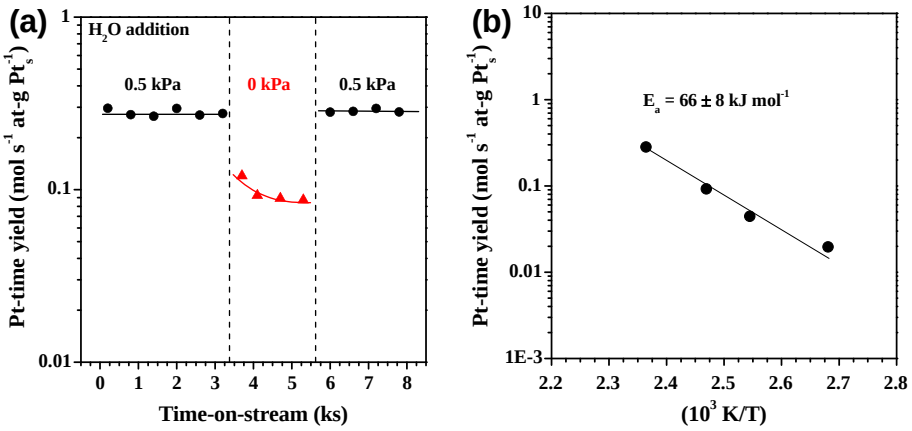

Fig. 11. H_2O effect on CO oxidation turnover rates (a, 423 K) and Arrhenius plot (b, 373–423 K) measured with Pt/Al_2O_3 (2.03% wt., 1.3 nm Pt clusters, 1 kPa CO, 10 kPa O_2). Symbols: (●) 0.5 kPa H_2O; (▲) 0 kPa H_2O.

Fig. 4 shows CO oxidation turnover rates (5 kPa CO, 2 kPa O_2, and 0.5 kPa H_2O) on Au/Al_2O_3 (3.5 nm Au) and Pt/Al_2O_3 (1.2 nm Pt) as a function of temperature. CO oxidation turnover rates were much higher on Au clusters than on Pt clusters. CO oxidation activation energies were also much smaller on Au/Al_2O_3 than Pt/Al_2O_3 (36 ± 3 versus 66 ± 8 kJ mol^{-1}). The lower CO oxidation rates on Pt clusters reflect CO*-saturated surfaces, a phenomenon that decreases O_2 adsorption rates on Pt [31]. In contrast, Au surfaces are not saturated with CO* intermediates during CO oxidation catalysis (as suggested by the small CO adsorption equilibrium, K_1). Consequently, the adsorption of O_2 and H_2O and the subsequent formation of the oxidant species (hydroperoxy intermediates) is more facile on Au-based catalysts.

3.8. Role of H_2O in CO oxidation pathways catalyzed by supported noble metal (Au, Pt) clusters

The experimental evidence reported here for H_2O effects on CO oxidation turnover rates resolves long-standing conflicts among measured rates on Au catalysts with similar cluster size, Au contents, supports, and synthetic provenance. The presence of H_2O as a co-catalyst in CO/O_2 reactants, even at trace concentrations, affects significantly catalyst stability and measured CO oxidation rates. H_2O addition is essential for stable turnover rates, and its presence leads to a sequence of elementary steps that are mediated by hydroperoxy species (*OOH), which account for the co-catalytic effect of H_2O on CO oxidation rates and on catalyst stability, as well as for the ability of Au clusters to catalyze propene epoxidation reactions with O_2/H_2O mixtures [28,59]. The elementary steps that form the hydroperoxy species from O_2 and H_2O occur exclusively on Au cluster surfaces without any significant involvement of support sites; hence, the reducible nature of the support become much less consequential for CO oxidation catalysis in the presence of the H_2O molecules that mediate required O_2 activation steps. In contrast, supports influence CO oxidation turnover rates with nominally anhydrous reactants, perhaps because they contribute either adsorbed H_2O that acts as co-catalyst in CO oxidation or periphery sites that become essential for O_2 activation, but which are required only in the absence of H_2O.

The observed H_2O effects in CO oxidation are not exclusive of reactions catalyzed by Au clusters. We find that H_2O also influences significantly measured CO oxidation rates with Pt clusters. This strongly suggests that CO oxidation with H_2O as a co-catalyst occurs on supported noble metal clusters via common elementary steps involving the formation of hydroperoxy species that are responsible for the higher measured CO oxidation rates compared to those with anhydrous CO/O_2 mixtures.

4. Conclusions

Moisture levels in "anhydrous" CO/O_2 streams well below the detection limits of typical speciation techniques are consequential for CO oxidation catalysis; this has led to our suggestion that the presence of H_2O is essential both for practical CO oxidation rates, for their reproducible measurements, and for fundamental studies of the mechanism and site requirements of these reactions. H_2O is an efficient co-catalyst necessary for O_2 activation steps and for catalyst stability in CO/O_2 reactions at near-ambient temperatures with Au clusters (<5 nm) deposited on reducible (TiO_2, Fe_2O_3) and non-reducible (Al_2O_3) supports. Rigorous kinetic and isotopic data measured on stable Au catalysts have led us to propose a mechanistic picture of CO oxidation in the presence of H_2O that involves H_2O-mediated O_2 activation steps that form hydroperoxy species (*OOH), which precisely account for the remarkable co-catalytic effect of H_2O on measured CO oxidation rates. These steps occur exclusively on the Au clusters; hence, the influence of support identity on CO oxidation catalysis, and specifically its reducible nature, becomes much less important in the presence of H_2O. These H_2O effects in CO/O_2 reactions are also found with Pt catalysts, which suggest that common elementary steps during $CO/O_2/H_2O$ reaction occurs on supported noble metal clusters (Au, Pt). The formation of hydroperoxy species explains the significantly higher CO oxidation rates compared to those measured with anhydrous CO/O_2 mixtures.

Acknowledgments

This work was supported by the Director, Office of Basic Energy Sciences, Chemical Sciences Division of the US Department of Energy under Contract DE-AC02-05CH11231. M. Ojeda acknowledges the financial support from the European Union (Marie Curie Actions, MOIF-CT2005-007651) and Spanish Ministry of Science and Innovation (RYC-2010-06067). H. Kung and M. Kung (Northwestern University) kindly provided the initial Au/Al_2O_3 catalysts and synthetic protocols. We thank Dr. David Flaherty for proofreading and helpful discussions. We are also grateful for the electron microscopy data provided by Dr. M. Avalos, L. Rendon and F. Ruiz from the *Centro de Ciencias de la Materia Condensada*, UNAM, Mexico. The World Gold Council (WGC) is also acknowledged for supplying the reference Au samples.

Appendix A

The rate of CO oxidation via the sequence of elementary steps shown in Scheme 1 is given by

$$r_{CO_2} = r_5 + r_7 \tag{A1}$$

By applying the pseudo-steady-state approximation (PSSA) to O* and *OH species, we find that $r_6 = r_7$ and $r_5/2 = r_6$, respectively. Consequently, Eq. (A1) becomes

$$r_{CO_2} = \frac{3}{2} r_5 = \frac{3}{2} k_5 [CO^*][^*OOH]/[L] \tag{A2}$$

where [L] is the number of active sites.

The *quasi*-equilibrium assumption for steps 1–4 gives

$$[CO^*] = K_1 P_{CO}[*] \tag{A3}$$

$$[O_2^*] = K_2 P_{O_2}[*] \tag{A4}$$

$$[H_2O^*] = K_3 P_{H_2O}[*] \tag{A5}$$

$$[^*OOH = \frac{K_4 [O_2^*][H_2O^*]}{[^*OH]} \tag{A6}$$

The PSSA to *OH gives

$$[^*OOH = \frac{2k_6 [OH]^2}{k_5 [CO^*]} \tag{A7}$$

Combining Eqs. (A3)–(A7)

$$[^*OH] = \left(\frac{K_1 K_2 K_3 K_4 K_5}{2k_6}\right)^{1/3} (P_{CO} P_{O_2} P_{H_2O})^{1/3} [*] \tag{A8}$$

Substituting Eq. (A8) in Eq. (A6)

$$[^*OOH] = \frac{(K_2 K_3 K_4)^{2/3} (2k_6)^{1/3}}{(K_3 K_5)^{1/3}} \frac{(P_{O_2} P_{H_2O})^{2/3}}{P_{CO}^{1/3}} [*] \tag{A9}$$

Hence, the rate of CO oxidation (Eq. (A2)) becomes

$$\begin{aligned} r_{CO_2} &= \frac{3}{2} (K_1 K_2 K_3 K_4 k_5)^{2/3} (2k_6)^{1/3} (P_{CO} P_{O_2} P_{H_2O})^{2/3} [*]^2/[L] \\ &= \alpha (P_{CO} P_{O_2} P_{H_2O})^{2/3} [*]^2/[L] \end{aligned} \tag{A10}$$

where

$$\alpha = \frac{3}{2} (K_1 K_2 K_3 K_4 K_5)^{2/3} (2k_6)^{1/3} \tag{A11}$$

[*OOH] and [*OH] can be written as follows:

$$[^*OOH] = \beta \frac{(P_{O_2} P_{H_2O})^{2/3}}{P_{CO}^{1/3}} [*] \tag{A12}$$

and

$$[^*OH] = \delta (P_{CO} P_{O_2} P_{H_2O})^{1/3} [*] \tag{A13}$$

where

$$\beta = \frac{(K_2 K_3 K_4)^{2/3} (2k_6)^{2/3}}{(K_1 k_5)^{1/3}} \tag{A14}$$

and

$$\delta = \left(\frac{K_1 K_2 K_3 K_4 K_5}{2k_6}\right)^{1/3} \tag{A15}$$

A site balance gives

$$[L] = [*] + [CO^*] + [O_2^*] + [H_2O^*] + [^*OOH] + [^*OH] + [O^*] \tag{A16}$$

Since $r_6 = r_7$,

$$\begin{aligned} [O^*] &= \frac{k_6 [^*OH]^2}{k_7 [CO^*]} = \frac{(K_2 K_3 K_4 k_5)^{2/3} k_6^{1/3}}{K_1^{1/3} (2)^{2/3} k_7} \frac{(P_{O_2} P_{H_2O})^{2/3}}{P_{CO}^{1/3}} [*] \\ &= \gamma \frac{(P_{O_2} P_{H_2O})^{2/3}}{P_{CO}^{1/3}} [*] \end{aligned} \tag{A17}$$

where

$$\gamma = \frac{(K_2 K_3 K_4 K_5)^{2/3} k_6^{1/3}}{K_1^{1/3} (2)^{2/3} k_7} \tag{A18}$$

The site balance can be also expressed as the following:

$$\begin{aligned} [L] = [*] + K_1 P_{CO}[*] + K_2 P_{O_2}[*] + K_3 P_{H_2O}[*] + \beta \frac{(P_{O_2} P_{H_2O})^{2/3}}{P_{CO}^{1/3}} \\ \times [*] + \delta (P_{CO} P_{O_2} P_{H_2O})^{1/3} [*] + \gamma \frac{(P_{O_2} P_{H_2O})^{2/3}}{P_{CO}^{1/3}} [*] \end{aligned} \tag{A19}$$

Therefore,

$$[*] = \frac{[L]}{1 + K_1 P_{CO} + K_2 P_{O_2} + K_3 P_{H_2O} + \beta \frac{(P_{O_2} P_{H_2O})^{2/3}}{P_{CO}^{1/3}} + \delta (P_{CO} P_{O_2} P_{H_2O})^{1/3} + \gamma \frac{(P_{O_2} P_{H_2O})^{2/3}}{P_{CO}^{1/3}}} \tag{A20}$$

Substituting Eq. (A20) in Eq. (A10)

$$r_{CO_2} = \frac{\alpha (P_{CO} P_{O_2} P_{H_2O})^{2/3}}{[1 + K_1 P_{CO} + K_2 P_{O_2} + K_3 P_{H_2O} + \beta \frac{(P_{O_2} P_{H_2O})^{2/3}}{P_{CO}^{1/3}} + \delta (P_{CO} P_{O_2} P_{H_2O})^{1/3} + \gamma \frac{(P_{O_2} P_{H_2O})^{2/3}}{P_{CO}^{1/3}}]^2} \tag{A21}$$

Appendix B. Supplementary data

Discussion on the CO oxidation kinetics corruptions imposed by H_2O condensation and concomitant mass transfer limitations inside the γ-Al_2O_3 pores; TEM images and Au cluster size distribution for the untreated and thermally-treated Au/Al_2O_3 samples; kinetic parameters obtained from nonlinear fitting to Eq. (1) of rate data measured with Au/Al_2O_3; kinetic dependence of CO oxidation turnover rates on CO pressure and O_2 pressure measured with the thermally treated Au/Al_2O_3 catalysts; and examples of alternate CO oxidation pathways, the derived kinetic expressions and the corresponding parity plots for the kinetic data measured with Au/Al_2O_3 (288 K; 0.80–8.25 kPa CO; 0.25–7.15 kPa O_2; 0.03–1.15 kPa H_2O). Supplementary data associated with this article can be found, in the online version, at doi:10.1016/j.jcat.2011.09.015.

References

[1] G.C. Bond, C. Louis, D.T. Thompson, Catalysis by Gold, Imperial College Press, London, 2006.
[2] B.K. Min, C.M. Friend, Chem. Rev. 107 (2007) 2709.
[3] T. Ishida, M. Haruta, Angew. Chem. Int. Ed. 46 (2007) 7154.
[4] M. Haruta, T. Kobayashi, H. Sano, N. Yamada, Chem. Lett. 16 (1987) 405.
[5] M.C. Kung, R.J. Davis, H.H. Kung, J. Phys. Chem. C 111 (2007) 11767.
[6] M.M. Schubert, S. Hackenberg, A.C. van Veen, M. Muhler, V. Plzak, R.J. Behm, J. Catal. 197 (2001) 113.
[7] G.C. Bond, D.T. Thompson, Gold Bull. 33 (2000) 41.
[8] C.J. Jia, Y. Liu, H. Bongard, F. Schüth, J. Am. Chem. Soc. 132 (2010) 1520.
[9] V. Aguilar-Guerrero, B.C. Gates, Catal. Lett. 130 (2009) 108.
[10] M. Daté, M. Haruta, J. Catal. 201 (2001) 221.
[11] F. Gao, T.E. Wood, D.W. Goodman, Catal. Lett. 134 (2010) 9.
[12] P. Landon, J. Fergusson, B.E. Solsona, T. Garcia, S. Al-Sayari, A.F. Carley, A.A. Herzing, C.J. Kiely, M. Makkee, J.A. Moulijn, A. Overweg, S.E. Golunski, G.J. Hutchings, J. Mater. Chem. 16 (2006) 199.
[13] H. Liu, A.I. Kozlov, A.P. Kozlova, T. Shido, Y. Iwasawa, Phys. Chem. Chem. Phys. 1 (1999) 2851.
[14] M. Daté, M. Okumura, S. Tsubota, M. Haruta, Angew. Chem. Int. Ed. 43 (2004) 2129.
[15] F. Boccuzzi, A. Chiorino, J. Phys. Chem. B 104 (2000) 5414.

[16] C.K. Costello, J.H. Yang, H.Y. Law, Y. Wang, J.N. Lin, L.D. Marks, M.C. Kung, H.H. Kung, Appl. Catal. A: Gen. 243 (2003) 15.
[17] Z. Wu, S. Zhou, H. Zhu, S. Dai, S.H. Overbury, J. Phys. Chem. C 113 (2009) 3726.
[18] W.C. Ketchie, M. Murayama, R.J. Davis, Topics Catal. 44 (2007) 307.
[19] K. Qian, W. Zhang, H. Sun, J. Fang, B. He, Y. Ma, Z. Jiang, S. Wei, J. Yang, W. Huang, J. Catal. 277 (2011) 95.
[20] H.H. Kung, M.C. Kung, C.K. Costello, J. Catal. 216 (2003) 425.
[21] V. Aguilar-Guerrero, B.C. Gates, J. Catal. 260 (2008) 351.
[22] C.K. Costello, M.C. Kung, H.S. Oh, Y. Wang, H.H. Kung, Appl. Catal. A: Gen. 232 (2002) 159.
[23] S.T. Daniells, A. Overweg, M. Makkee, J.A. Moulijn, J. Catal. 230 (2005) 52.
[24] S.D. Lin, M. Bollinger, M.A. Vannice, Catal. Lett. 17 (1993) 245.
[25] M.A. Bollinger, M.A. Vannice, Appl. Catal. B: Environ. 8 (1996) 417.
[26] C.G. Long, J.D. Gilbertson, G. Vijayaraghavan, K.J. Stevenson, C.J. Pursell, B.D. Chandler, J. Am. Chem. Soc. 130 (2008) 10103.
[27] D.G. Barton, S.G. Podkolzin, J. Phys. Chem. B 109 (2005) 2262.
[28] M. Ojeda, E. Iglesia, Chem. Commun. (2009) 352.
[29] M. Ojeda, E. Iglesia, Angew. Chem. Int. Ed. 48 (2009) 4800.
[30] E.P. Barrett, L.G. Joyner, P.P. Halenda, J. Am. Chem. Soc. 73 (1951) 373.
[31] A.D. Allian, K. Takanabe, K.L. Fujdala, X. Hao, T.J. Truex, J. Cai, C. Buda, M. Neurock, E. Iglesia, J. Am. Chem. Soc. 113 (2011) 4498.
[32] C.K. Costello, J. Guzman, J.H. Yang, Y.M. Wang, M.C. Kung, B.C. Gates, H.H. Kung, J. Phys. Chem. B 108 (2004) 12529.
[33] J.A. Biscardi, E. Iglesia, J. Catal. 182 (1999) 117.
[34] J.T. Calla, R.J. Davis, Ind. Eng. Chem. Res. 44 (2005) 5403.
[35] E. Quinet, L. Piccolo, F. Morfin, P. Avenier, F. Diehl, V. Caps, J.L. Rousset, J. Catal. 268 (2009) 384.
[36] M. Olea, M. Tada, Y. Iwasawa, J. Catal. 248 (2007) 60.
[37] J.T. Calla, M.T. Bore, A.K. Datye, R.J. Davis, J. Catal. 238 (2006) 458.
[38] T.V. Choudhary, C. Sivadinarayana, C.C. Chusuei, A.K. Datye, J.P. Fackler, D.W. Goodman, J. Catal. 207 (2002) 247.
[39] E. Quinet, F. Morfin, F. Diehl, P. Avenier, V. Caps, J.L. Rousset, Appl. Catal. B: Environ. 80 (2008) 195.
[40] Z.P. Liu, P. Hu, A. Alavi, J. Am. Chem. Soc. 124 (2002) 14770.
[41] A. Bongiorno, U. Landman, Phys. Rev. Lett. 95 (2005) 106102.
[42] C.R. Chang, Y.G. Wang, J. Li, Nano Res. 4 (2011) 131.
[43] M. Neurock, A. Wieckowski, Adv. Phys. Chem., in press.
[44] M. Boudart, G. Djéga-Mariadassou, Kinetics of Heterogeneous Catalytic Reactions, Princeton University Press, Princeton, 1984.
[45] C. Shang, Z.P. Liu, J. Phys. Chem. C 114 (2010) 16989.
[46] N. Lopez, J.K. Norskov, J. Am. Chem. Soc. 124 (2002) 11262.
[47] M. Mavrikakis, P. Stoltze, J.K. Norskov, Catal. Lett. 64 (2000) 101.
[48] T. Yan, J. Gong, D.W. Flaherty, C.B. Mullins, J. Phys. Chem. C 115 (2011) 2057.
[49] B. Schumacher, Y. Denkwitz, V. Plzak, M. Kinne, R.J. Behm, J. Catal. 224 (2004) 449.
[50] D. Widmann, Y. Liu, F. Schüth, R.J. Behm, J. Catal. 276 (2010) 292.
[51] M. Haruta, S. Tsubota, T. Kobayashi, H. Kageyama, M.J. Genet, B. Delmon, J. Catal. 144 (1993) 175.
[52] G. Li, J. Edwards, A.F. Carley, G.J. Hutchings, Catal. Today 114 (2006) 369.
[53] M. Okumura, Y. Kitagawa, K. Yamaguchi, T. Akita, S. Tsubota, M. Haruta, Chem. Lett. 32 (2003) 822.
[54] B. Chowdhury, J.J. Bravo-Suarez, N. Mimura, J. Lu, K.K. Bando, S. Tsubota, M. Haruta, J. Phys. Chem. Lett. 110 (2006) 22995.
[55] C. Sivadinarayana, T.V. Choudhary, L.L. Daemen, J. Eckert, D.W. Goodman, J. Am. Chem. Soc. 126 (2003) 38.
[56] B. Taylor, J. Lauterbach, G.E. Blau, W.N. Delgass, J. Catal. 242 (2006) 142.
[57] P. Landon, P.J. Collier, A.J. Papworth, C.J. Kiely, G.J. Hutchings, Chem. Commun. 18 (2002) 2058.
[58] C. Rossignol, S. Arrii, F. Morfin, L. Piccolo, V. Caps, J.L. Rousset, J. Catal. 230 (2005) 476.
[59] J. Jiang, S.M. Oxford, B. Fu, M.C. Kung, H.H. Kung, J. Ma, Chem. Commun. 46 (2010) 3791.
[60] L. Piccolo, H. Daly, A. Valcarcel, F.C. Meunier, Appl. Catal. B: Environ. 86 (2009) 190.
[61] M. Shou, H. Takekawa, D.Y. Ju, T. Hagiwara, D.L. Lu, K.I. Tanaka, Catal. Lett. 108 (2006) 119.
[62] S. Alayoglu, A.U. Nilekar, M. Mavrikakis, B. Eichhorn, Nat. Mater. 7 (2008) 333.
[63] R.H. Nibbelke, M.A.J. Campman, J.H.B.J. Hoebink, G.B. Marin, J. Catal. 171 (1997) 358.
[64] J. Bergeld, B. Kasemo, D.V. Chakarov, Surf. Sci. 495 (2001) L815.
[65] P. Panagiotopoulou, D.I. Kondarides, Catal. Today 112 (2006) 49.